Time- and Space-Resolved Flow-Cytometry of Cell Organelles to Quantify Nanoparticle Uptake and Intracellular Trafficking by Cells

Garcia Romeu, Hector; Deville, Sarah; Salvati, Anna

Published in:
Small

DOI:
10.1002/smll.202100887

Publication date:
2021

NANO · MICRO small
www.small-journal.com

Time- and Space-Resolved Flow-Cytometry of Cell Organelles to Quantify Nanoparticle Uptake and Intracellular Trafficking by Cells

*Hector Garcia Romeu, Sarah Deville, and Anna Salvati**

The design of targeted nanomedicines requires intracellular space- and time-resolved data of nanoparticle distribution following uptake. Current methods to study intracellular trafficking, such as dynamic colocalization by fluorescence microscopy in live cells, are usually low throughput and require extensive analysis of large datasets to quantify colocalization in several individual cells. Here a method based on flow cytometry to easily detect and characterize the organelles in which nanoparticles are internalized and trafficked over time is proposed. Conventional cell fractionation methods are combined with immunostaining and high-sensitivity organelle flow cytometry to get space-resolved data of nanoparticle intracellular distribution. By extracting the organelles at different times, time-resolved data of nanoparticle intracellular trafficking are obtained. The method is validated by determining how nanoparticle size affects the kinetics of arrival to the lysosomes. The results demonstrate that this method allows high-throughput analysis of nanoparticle uptake and intracellular trafficking by cells, therefore it can be used to determine how nanoparticle design affects their intracellular behavior.

1. Introduction

Nano-sized materials are used for improving the delivery of drugs to their target, thanks to their unique ability to exploit cellular mechanisms to enter and distribute into cells and organisms.[1–3] In order to improve nanomedicine targeting and efficacy, precise control of nanoparticle behavior and fate at cellular level is required. To this aim, detailed data of nanoparticle uptake, intracellular trafficking and intracellular distribution kinetics are required in order to determine how nanoparticle properties and design can be engineered in order to control nanoparticle outcomes at the cell level. The current approaches to study the internalization and trafficking of nanoparticles typically are based on dynamic colocalization in cell organelles by live-cell confocal fluorescence microscopy.[4,5] Due to the limits of resolution in light microscopy, a spatial overlap in fluorescence imaging does not necessarily indicate colocalization. As a result, precise colocalization in cells by live-imaging requires particle tracking[6] and correlated movement of object trajectories in 3 dimensions, as well as specific algorithms to determine and quantify colocalization.[7] In addition, it is necessary to account for cell variability by analyzing dozens of cells multiple times. Thus, although such imaging-based methods offer several advantages, such as high spatial resolution and the possibility to study heterogeneity across individual cells, they do require extensive data and statistical analysis to determine nanoparticle trafficking in specific cell organelles over time.

As an improvement to standard light microscopy, many novel super-resolution microscopy methods have been developed, such as super-resolution structured illumination microscopy,[8] photoactivation localization microscopy,[9,10] and stimulated emission depletion microscopy.[11,12] However, these methods produce extensive amounts of data per cell as well, resulting-again-in relatively complex and often low-throughput analyses. Thus, alternative colocalization methods are required to expedite the quantification of nanoparticle intracellular distribution over time and to screen multiple material designs with ease.

Flow cytometry is a high-throughput method commonly available in most laboratories and routinely used to analyze large populations of cells on an individual cell basis. One main drawback in comparison to image-based methods is that flow cytometry lacks spatial (intracellular) resolution. However, thanks to the latest technological developments, nowadays flow cytometry can detect particles as small as 100–200 nanometers,

H. Garcia Romeu, Dr. S. Deville,[+] Prof. A. Salvati
Department of Nanomedicine & Drug Targeting
Groningen Research Institute of Pharmacy
University of Groningen
A. Deusinglaan 1, Groningen 9713AV, The Netherlands
E-mail: a.salvati@rug.nl
Dr. S. Deville
Health Unit
Flemish Institute for Technological Research
Boeretang 200, Mol 2400, Belgium

The ORCID identification number(s) for the author(s) of this article can be found under https://doi.org/10.1002/smll.202100887.

[+]Present address: Laboratory of Experimental Cancer Research, Department of Human Structure and Repair, Ghent University, 9000 Ghent, Belgium

DOI: 10.1002/smll.202100887

including cell organelles.[13] This has allowed the introduction of single organelle flow analysis (sometimes referred to as "SOFA"), which has been used to study different organelles such as endosomes,[14] lysosomes,[15] mitochondria,[16] and autophagic vacuoles.[17] Similarly, in recent years, high-sensitivity flow cytometry has become one of the main methods to characterize extracellular vesicles, and has also been applied to the characterization of viruses and nanoparticles.[13,18–23]

Within this context, here we show how high-sensitivity organelle flow cytometry can be applied to generate space- and time-resolved data of nanoparticle intracellular distribution and obtain in this way nanoparticle intracellular distribution kinetics. By taking advantage of the relatively large size of fluorescently labeled nanoparticles in comparison to—for instance—labeled proteins, the organelles containing nanoparticles can be easily detected and analyzed by flow cytometry. Thus, cells are exposed to fluorescently labeled nanoparticles, then the organelles are extracted by conventional fractionation methods and characterized by high-sensitivity flow cytometry. This allows to analyze the organelles recovered from several thousands of cells per sample and characterize those containing nanoparticles in high-throughput. By immunostaining the organelles, information on nanoparticle colocalization into specific organelles can be obtained, and by extracting the organelles at different times after nanoparticle uptake, the kinetics of intracellular trafficking can be readily determined. In this way, organelle flow cytometry allows to obtain space- and time-resolved data to map nanoparticle uptake and intracellular trafficking. Determining nanoparticle intracellular distribution and kinetics can help to tune their design for specific applications, overall contributing to the development of targeted nanomedicines.

2. Results

Human cancer epithelial HeLa cells and yellow-green fluorescently labeled carboxylated polystyrene (PS-COOH) nanoparticles of 40, 100, and 200 nm were selected as common cell and nanoparticle models for which extensive information is already available.[24–26] Nevertheless, any other cell type could be used, as also other fluorescently-labeled nanoparticles, provided their signal is strong enough to allow detection in the isolated organelles. Nanoparticle characterization by dynamic light scattering (DLS) and zeta potential measurements confirmed that for all nanoparticle sizes homogenous dispersions could be obtained, both in phosphate buffered saline (PBS) and in the cell culture medium with serum used for cell studies (**Table 1** and Figure S1, Supporting Information, for the corresponding size distributions). For the dispersions in cell culture medium with serum, the average diameter increased as commonly observed upon absorption of proteins on the nanoparticles and corona formation. As a first step, we optimized the flow cytometry settings for the detection of nano-sized objects, and the organelle extraction method to preserve organelle integrity.

2.1. Setting up the Flow Cytometer to Measure Nano-Sized Objects

When using conventional flow cytometers, measuring nano-sized objects can be challenging depending on the limits of detection of the instrument. However, some flow cytometers offer setups with higher sensitivity for the detection of objects in the nanoscale. In some instruments, this is achieved by using a violet laser (405 nm) to detect side scattering, as opposed to the standard 488 nm laser (using light at lower wavelength improves resolution[27]). In all cases, optimization of the measurement settings is required to set up flow cytometry in high sensitivity mode. To this aim, we adapted the protocol from Spittler et al.[28] In brief, the side scattering (SSC) from a violet laser (405 nm, VSSC) is used to set the minimum threshold required for the events to be detected, and polystyrene green fluorescent calibration nano-beads are measured to fix the voltage gains. Figure S2A, Supporting Information, shows that in this way the seven populations of the calibration beads (100, 160, 200, 240, 300, 500, and 900 nm) are well separated in a dot plot (VSSC versus green fluorescence intensity (fluorescein isothiocyanate channel (FITC)). We also tested the SSC from the blue laser (488 nm, BSSC) and the forward scattering (FSC). In the BSSC channel the smallest population (100 nm) could not be detected (Figure S2B,

Table 1. Nanoparticle physico-chemical characterization by DLS and zeta potential measurements. Yellow-green fluorescent PS-COOH nanoparticles are dispersed in PBS or MEM cell culture medium supplemented with 10% FBS (cMEM) at a concentration of 100 μg mL^{-1}. The dispersions in cMEM are incubated for 1 h shaking at 37 °C prior to measurement. For each sample, a total of three replicate measurements of five runs each are made. The table shows the average and standard deviation of the values obtained from the three replicate measurements. The data confirmed that for all nanoparticles homogenous dispersions are obtained both in PBS and in the cell medium with serum used for experiments with cells. A slight increase in size is observed in the presence of serum. Finally, the zeta potential is negative for all the samples, as expected due to the presence of carboxylated groups on the nanoparticle surface. In the presence of serum, the zeta potential decreases towards neutrality, as expected upon formation of a protein corona on the nanoparticles.

Size	Medium	Diameter [Z-average, nm][a)]	PDI[a)]	Diameter [nm][b)]	Zeta potential [mV]
40 nm	PBS	57 ± 0	0.18 ± 0.00	62 ± 1	−30 ± 1
	cMEM[c)]	–	–	107 ± 1	−8 ± 0
100 nm	PBS	112 ± 0	0.02 ± 0.02	121 ± 2	−37 ± 0
	cMEM[c)]	–	–	161 ± 1	−7 ± 0
200 nm	PBS	186 ± 1	0.02 ± 0.01	207 ± 1	−36 ± 0
	cMEM[c)]	–	–	251 ± 6	−7 ± 0

[a)]Z-average diameter and polydispersity index (PDI) obtained by cumulant analysis of DLS data; [b)]Diameter obtained by CONTIN analysis from the size distributions shown in Figure S1, Supporting Information; [c)]For the samples in cMEM, the size distributions obtained by CONTIN analysis are shown in Figure S1, Supporting Information.

Supporting Information). Similarly, in the FSC channel only the biggest populations could be distinguished (500 and 900 nm) (Figure S2D, Supporting Information). Given that the VSSC allows to detect objects as small as 100 nm (note that this also depends on the material, since the side scattering increases with both the size and the refractive index of the material), the detection threshold was applied on the VSSC channel.

Flow cytometers can also be triggered in a specific fluorescence channel as we show in Figure S2C, Supporting Information, for the FITC-channel. This could be necessary, for instance, for fluorescent nano-sized objects with VSSC below the threshold. However, if this configuration is used, only fluorescent objects are detected and all other objects are missed. Therefore, this configuration could be used as an inclusive logical operator (OR) in conjunction with the VSSC threshold. This means that an event is detected as long as it has enough scattering or fluorescence to surpass either one of the two thresholds (VSSC or FITC threshold). Finally, we tested the calibration beads in a flow cytometer that did not offer any high sensitivity set up for comparison. In this case, only the largest nano-beads (300, 500, and 900 nm) were detected as distinct populations (Figure S2E, Supporting Information).

Other important settings that need to be optimized in high-sensitivity flow cytometry are those to avoid the so-called "swarm detection". A swarm can be generated when more than one object is detected as a single event by the flow cytometer, causing false positives and underestimation of event counts.[29] This is not a common issue when using a standard configuration. However, it can occur when pushing flow cytometry to measure objects at the detection limit. The best way to avoid swarm detection is to measure the same sample at different dilutions, and set the dilution and flow rate at a range where the number of events measured is proportional to the dilution.[28] The best working range in our system was between 1500 and 4000 events per second (eps) (Figure S3A, Supporting Information). Measurements faster than 4000 eps would cause high swarm detection and underestimation of our sample (Figure S3B, Supporting Information). On the other hand, measurements slower than 1000 eps would include a high contribution of background events (>10%) (Figure S3C, Supporting Information).

2.2. Detection of Organelles Containing Nanoparticles by Flow Cytometry

The workflow in **Figure 1** displays the procedure followed to extract organelles from Hela cells. In brief, a basic fractionation is performed to remove bigger objects (such as nuclei and cell debris), as well as the smaller objects, such as the cytosolic proteins (as explained in more detail in the Experimental Section). As a result, a mixture of all different cell organelles is obtained, thus including the organelles in which nanoparticles are trafficked. When measuring PBS some background events were recorded, as expected when lowering the detection threshold (**Figure 2**A). With the optimized settings, the event rate for PBS was usually around 200 eps. Similarly, the flow cytometer could detect the unlabeled organelles isolated from untreated Hela cells (Figure 2B), but since they did not have any fluorescent label, their fluorescence was comparable to the PBS background. Because of this, the amount of non-fluorescent events recorded from the sample of unlabeled organelles (Figure 2B) was much higher than what observed for PBS (Figure 2A). When directly measuring a dispersion of the fluorescent nanoparticles in PBS (Figure S4, Supporting Information) or in the cell culture medium supplemented with serum (Figure 2C), the 100 and 200 nm nanoparticles could be detected and resolved well, with the full population above the threshold. Only the 40 nm nanoparticles did not have high enough scattering in the VSSC channel to pass the detection threshold, so for this sample, an additional inclusive threshold (logical operator "OR") in their fluorescence channel (FITC) was added. In this way, events with low VSSC but high enough fluorescence in the FITC channel could still be detected. We also note the slightly higher background of non-fluorescent events for the nanoparticles in cell culture medium (Figure 2C) in comparison to the nanoparticle dispersions in PBS (Figure S4, Supporting Information), due to the presence of the (unlabeled) free proteins in solution. As a further test on the detection limits, we counted the nanoparticles in a sample at a known concentration. The detection was close to 100% for the bigger sizes (100 and 200 nm) and around 50% for the 40 nm nanoparticles (Figure S5, Supporting Information).

Finally, in the case of organelles extracted from Hela cells exposed to the different nanoparticles (Figure 2D), for all nanoparticles sizes, next to the high amount of non-fluorescent organelles recovered from cells, a clear population of fluorescent objects could be detected, with a strong shift in the VSSC channel when compared to the free nanoparticles, as expected for organelles containing nanoparticles. Again, only the organelles containing 40 nm nanoparticles could not be fully separated from the background.

2.3. Optimization of the Organelle Extraction

Another aspect to optimize next to sensitivity and swarm detection is the method of organelle extraction. The organelles must

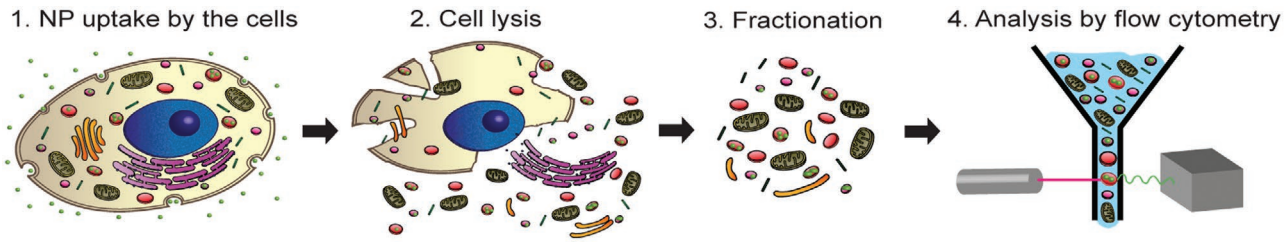

Figure 1. Scheme of the method developed in this study for organelle flow cytometry. In brief, 1) Hela cells are incubated with fluorescent nanoparticles, 2) lysed, and 3) the organelles are extracted using standard fractionation methods. Finally, 4) the organelles are individually measured by flow cytometry.

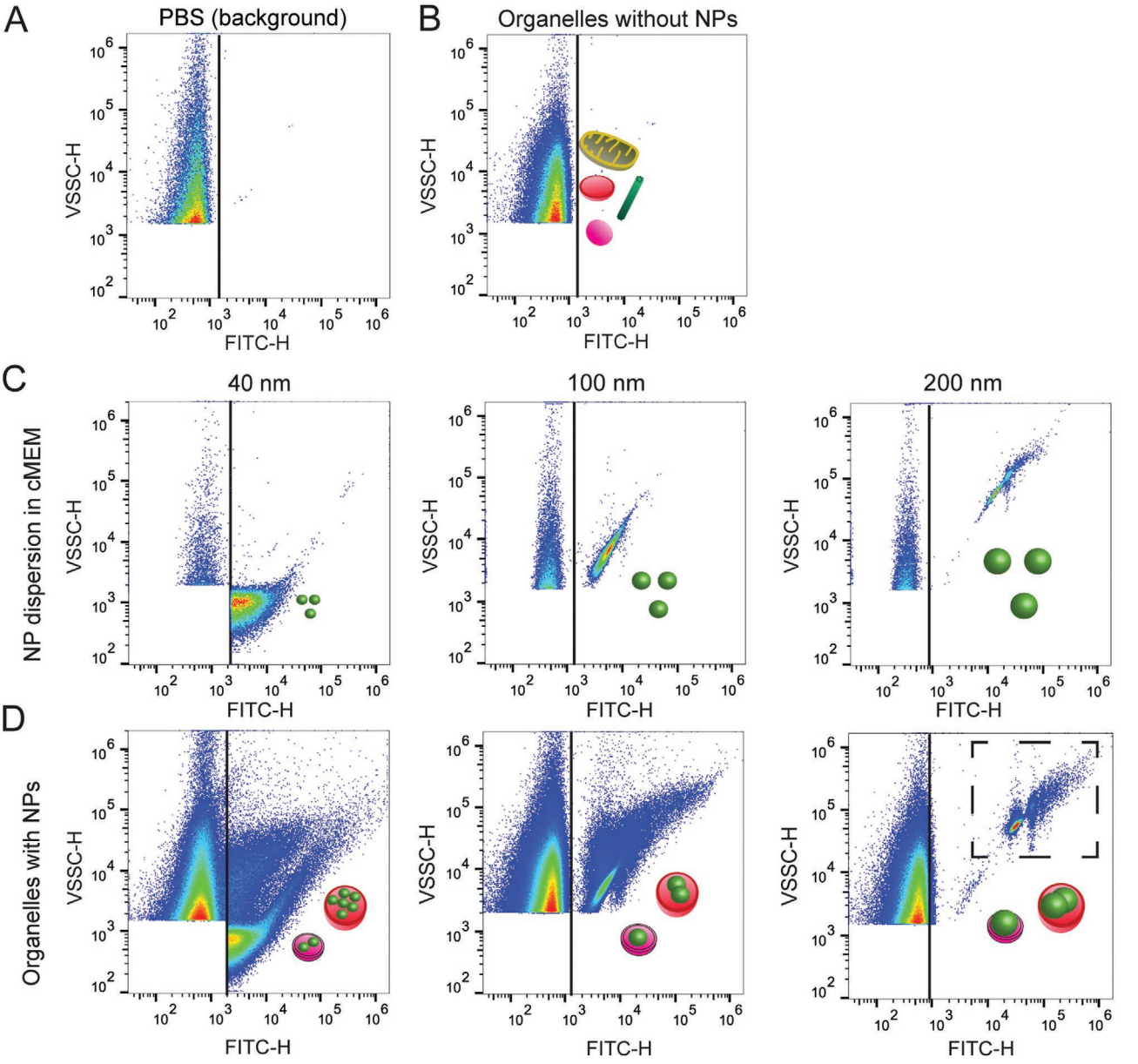

Figure 2. High-sensitivity flow cytometry of nanoparticles and cell organelles. A–D) Dot plots showing the Violet SSC and FITC fluorescence of background events from PBS (A), unlabeled organelles extracted from untreated Hela cells (B), dispersions of the fluorescent yellow-green PS-COOH nanoparticles of different sizes (5, 20, and 50 ng mL^{-1}, for the 40, 100, and 200 nm nanoparticles, respectively) in cell culture medium supplemented with serum (C) and organelles from Hela cells exposed for 24 h to 10, 25, and 50 µg mL^{-1} of the 40, 100, and 200 nm nanoparticles, respectively (D). Nanoparticles as small as 40 nm can be detected and counted and the populations of organelles containing fluorescent nanoparticles bigger than 100 nm can be fully separated from the rest of the organelles.

be intact to avoid leaking of free nanoparticles, which would lead to an underestimation of their colocalization.

It is known that most nanoparticles enter via endocytosis and go to lysosomes.[4,24,25] Thus, here, as a first step, we focused on the lysosomes to optimize the extraction protocols. Two different methods were compared, namely cell lysis using either a Potter-Elvehjem homogenizer or crystal beads.[30] Then, in order to test organelle integrity, we used two different antibodies against the lysosome-associated (trans)membrane protein 1 (LAMP1) (**Figure 3**A), an antibody for its cytosolic portion (clone H50), and another one which specifically binds to its lumenal (intralysosomal) portion (clone H43). First of all, the results showed that specific organelles, in this case, the lysosomes, could be stained and distinguished from the rest of the organelles, confirming the suitability of the method for colocalization studies (Figures 3–4). Additionally, by using an antibody for the lumenal portion of LAMP1, lysosomes damaged during the extraction (thus allowing accumulation of the antibody) could be distinguished. The dot plots in Figure 3B show a higher percentage of damaged lysosomes after extraction using crystal beads. Furthermore, the percentage of damaged lysosomes increased when using an increasing

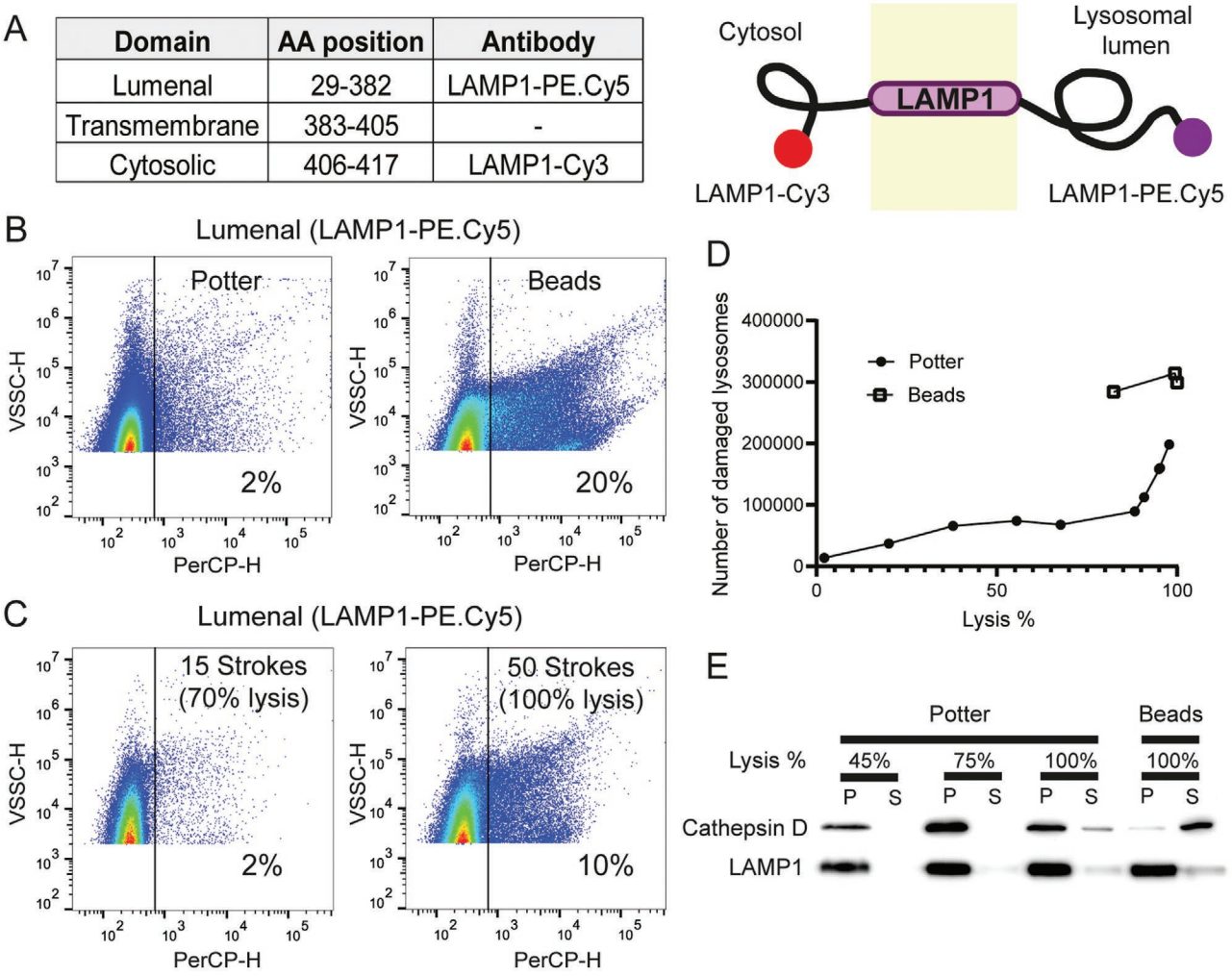

Figure 3. Optimization of organelle extraction. A) Table and scheme showing the localization of the amino acids of LAMP1 protein in the lysosome, and the epitopes of the different LAMP1 antibodies used. B–E) Flow cytometry double scatter plots of organelles immunostained against lumenal LAMP1 to detect damaged lysosomes. B) Organelles extracted using the Potter-Elvehjem homogenizer (Potter) or crystal beads (Beads). Immunostaining shows that when using crystal beads a higher number of damaged organelles stained for lumenal LAMP1 is detected (the fluorescence signal of this labeled antibody is detected in the PerCP (Peridinin-Chlorophyll-Protein) channel). C) Organelles extracted using the Potter-Elvehjem homogenizer after applying a different number of strokes. The dot plot shows that increasing the number of strokes performed results in higher lysis percentages, but also a higher number of damaged organelles. D) Number of damaged lysosomes as a function of the cell lysis percentage for the Crystal Beads and Potter-Elvehjem homogenizer lysis methods. Performing cell lysis in percentages higher than 90% resulted in a high number of damaged lysosomes. E) Western Blot for Cathepsin D and LAMP1 on organelles extracted from Hela cells with the Potter-Elvehjem homogenizer at 3 different lysis percentages (45, 75, and 100%) or with crystal beads (100% lysis). All samples are centrifuged at 20.000 g to pellet the lysosomes, and for each sample, both the pellet (P) and supernatant (S) obtained in this way are analyzed by western blot. The results show that when using the crystal beads and at high lysis percentages higher amount of Cathepsin D is released in the supernatant, thus higher damage to the lysosomes is observed.

number of strokes in the extraction with the homogenizer (Figure 3C, for a different experiment with the homogenizer, where different number of strokes were used). Thus, when lysing more cells, more organelles could be recovered, but the number of damaged organelles also increased (Figure S6, Supporting Information). When comparing the integrity of the organelles recovered with the two methods at the same cell lysis percentage (Figure 3D), the results showed that the number of damaged lysosomes was 10 times higher when using crystal beads. Organelle integrity was also checked by western blotting of cathepsin D, a small free protein (25 kDa) found inside the lysosomes (Figure 3E). After cell lysis, lysosomes were pelleted by centrifugation for 20 min at 20 000 g. Thus, if the lysosomes were damaged, the cathepsin would be released and found in the supernatant. In line with the flow cytometry results, the western blot confirmed that increasing cell lysis percentage to 100% led to release of cathepsin D in the supernatant, indicative of organelle damage, and that overall the damage was stronger for cells lysed using crystal beads.

Based on all these results, all further extractions were performed using the homogenizer and keeping cell lysis in the range of 65–85%. **Figure 4**A shows the organelles immunostained with both types of LAMP1 antibodies after following the optimized organelle extraction protocol. The results

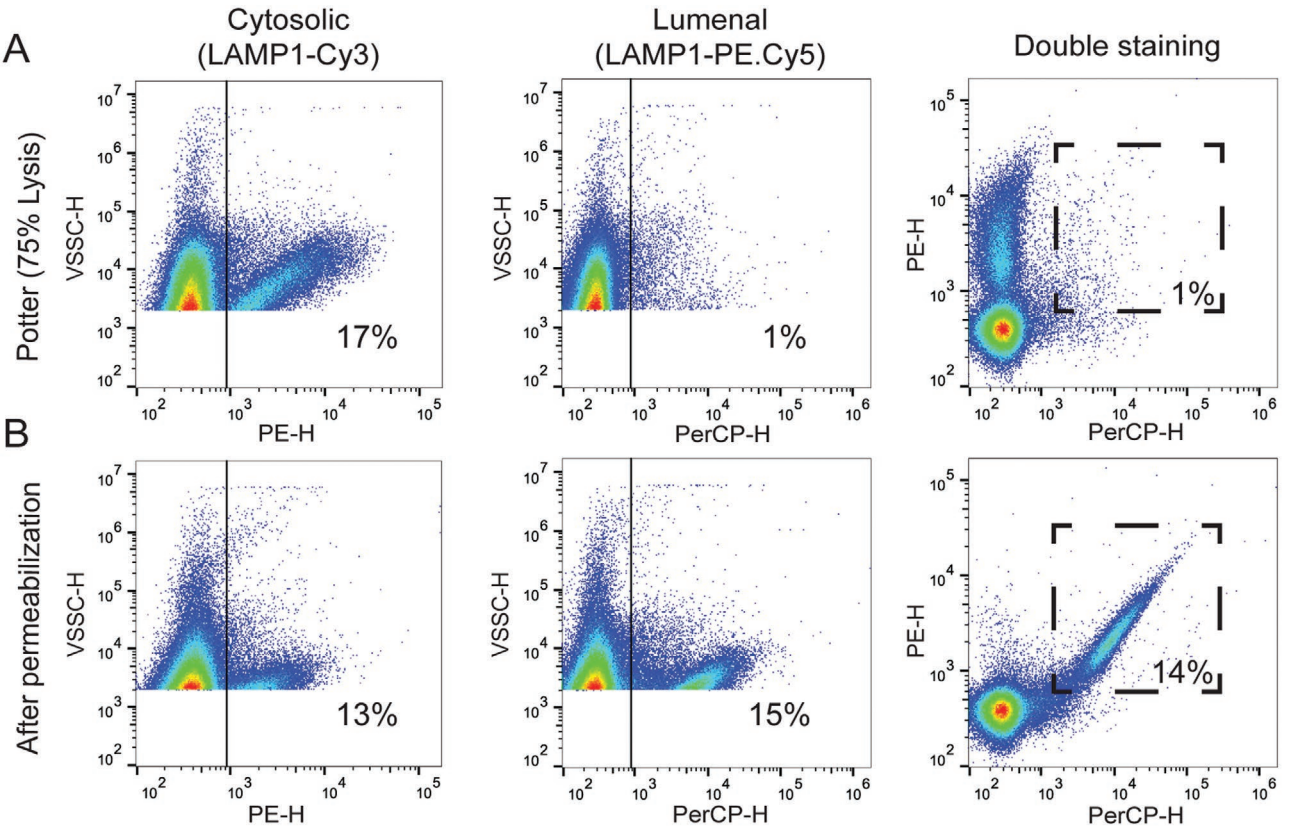

Figure 4. Immunostaining of the lumenal and cytosolic epitopes of the lysosomal protein LAMP1 to determine organelle integrity. A–B) Flow cytometry double scatter plots of violet side scattering (VSSC) and fluorescence of organelles immunostained using two LAMP1 antibodies, one against a cytosolic epitope (phycoerythrin (PE) channel) and one against a luminal epitope (PerCP channel). The organelles are extracted using the optimized method (Potter-Elvehjem homogenizer 75% lysis) and measured by flow cytometry without (A) and with permeabilization (B). With the optimized method, the number of damaged lysosomes stained by the lumenal antibody against LAMP1 is very low. After organelle permeabilization instead, all the lysosomes are damaged, thus stained by both antibodies. The double-staining observed after permeabilization also confirms the specificity of the antibodies against the lysosomes. The numbers inside the dot plots indicate the percentage of stained lysosomes inside the gate selected with the vertical line or within the dashed line.

confirmed that with the optimized methods, lysosomes stained with the cytosolic antibody could be distinguished well from the rest of the organelles, whereas staining by the lumenal LAMP1 antibody was practically absent. As a further control, the organelles were permeabilized and in this way, as expected, all detected lysosomes were stained by both antibodies (Figure 4B).

2.4. Quantification of Nanoparticle Colocalization in Different Organelles by Flow Cytometry

Most nanoparticles, including those used for this study, are known to enter by some form of active endocytosis, pass through endosomes, and finally accumulate in the lysosomes.[4,24,25] Therefore, in order to validate the method, we used organelle flow cytometry to determine the kinetics of nanoparticle trafficking via the endosomes and accumulation into the lysosomes.

After organelle extraction, the endosomes were labeled with an antibody against the endosomal protein EEA1 (Early Endosome Antigen 1) and in a separate experiment, the lysosomes were labeled with the cytosolic antibody against LAMP1. We then used size exclusion chromatography to wash away residual free antibody and elute all organelles in different volume fractions. Figure S7, Supporting Information, shows as an example the results obtained for all fractions recovered from a sample with lysosomes labeled with the cytosolic antibody against LAMP1. By measuring each fraction by flow cytometry, the fractions where the organelles containing the nanoparticles were found could be identified (Figure S7A, Supporting Information). Fluorescence measurements and protein quantification of all fractions confirmed removal of the excess free antibody and cytosolic free proteins (Figure S7B,C, Supporting Information).

Thus, the same procedure was used for HeLa cells exposed to 100 nm PS-COOH nanoparticles for 30 min (pulse), followed by nanoparticle removal and extraction of cell organelles at different times (0-to-5-h chase). All samples were prepared in the same way and acquired for the same time in order to determine how the percentage of nanoparticle colocalization with the endosome or lysosomes varied over time. In this way, the kinetics of nanoparticle trafficking through the endosomes and accumulation into the lysosomes could be determined (**Figure 5**). By plotting the nanoparticle fluorescence (FITC) versus the endosome fluorescence (PE, Figure 5A) or lysosome

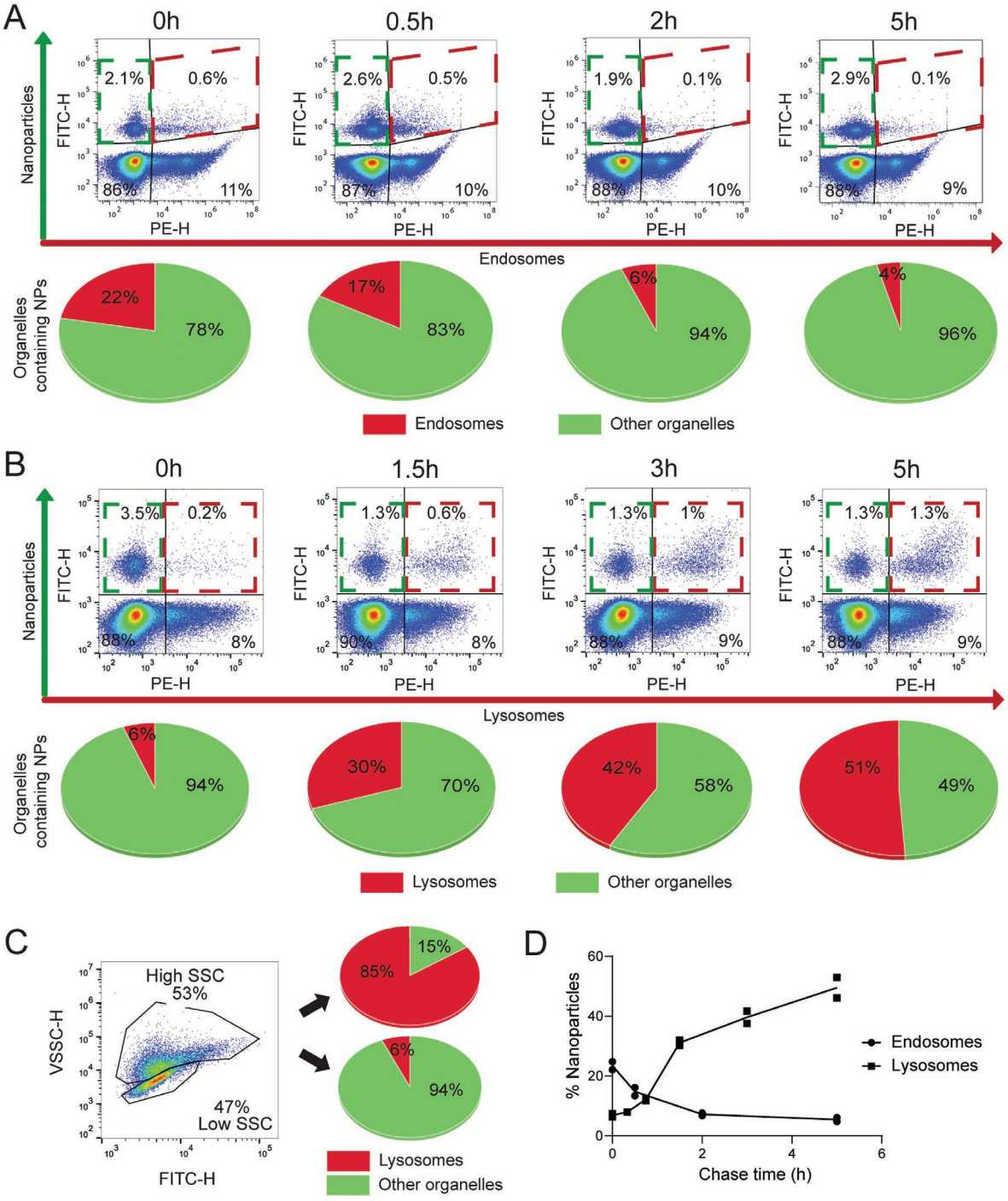

Figure 5. Kinetics of nanoparticle trafficking through the endosomes and accumulation into the lysosomes. A–B) Pulse and chase study of the trafficking of fluorescent yellow-green 100 nm PS-COOH nanoparticles to the endosomes and the lysosomes. Double scatter plots of nanoparticle (FITC) and A) endosome or B) lysosome (PE) fluorescence of the organelles recovered from Hela cells exposed for 30 min (Pulse) to 100 μg mL^{-1} nanoparticles, and then chased for different times after removal of the extracellular nanoparticles (Chase). The organelles are immunostained for EEA1 (A) or LAMP1 (B) (PE-H) to quantify the percentage of endosomes or lysosomes, respectively (Red), and all other organelles containing nanoparticles (Green). C) Dot plot of the organelles and LAMP1-stained lysosomes containing nanoparticles recovered after 5-h chase. Two populations can be distinguished in the VSCC fluorescence channel (high SSC and low SSC as indicated by the polygonal gates), with a very different fraction of nanoparticles in the lysosomes, as quantified for each population in the pie charts. D) Fraction of nanoparticles in the endosomes and lysosomes after 30-min pulse and different chase times up to 5 h, extracted from the data of panels A and B. After 30 min exposure, the fraction of nanoparticles in the endosomes decreases over time, and the fraction of those in the lysosomes increases, as the nanoparticles are trafficked through the endosomes towards the lysosomes. The numbers included inside the dot plots and pie charts indicate the fraction of events over the total. In C and D, the total number of objects measured in all organelle fractions recovered from 2 replicate samples is shown together with a line that passes through their average.

fluorescence (PE, Figure 5B), four populations of organelles can be distinguished: endosomes or lysosomes with and without nanoparticles (PE +, FITC + and PE + FITC −, respectively), organelles other than the endosomes or lysosomes containing nanoparticles (PE −, FITC +), and all other organelles without nanoparticles (PE −, FITC −). The results showed that after a 30-min pulse (0-h chase), around 25% of the organelles containing the 100 nm nanoparticles were endosomes (Figure 5A) and only 5% were lysosomes (Figure 5B). Then, as the chase time increased, nanoparticle colocalization in the endosomes decreased down to 5% while nanoparticle colocalization with the lysosomes increased up to ≈50%. In line with these results, Sandin et al.[25] used live-cell microscopy to determine nanoparticle colocalization in HeLa cells and showed that the same 100 nm PS-COOH nanoparticles first transited through Rab5-stained endosomes (with colocalization up to ≈25% maximum at comparable timescales), then accumulated into LAMP1-stained lysosomes, reaching on average 50–60% colocalization after 3-h chase (the result varying for individual cells).

Interestingly, in the case of the lysosomes, the high sensitivity of the VSSC also allowed us to distinguish 2 populations in the 5-h chase sample (Figure 5C), offering an extra degree of analysis. One population had higher VSSC and 85% colocalization of the nanoparticles in the lysosomes, whereas the second population with lower VSSC only had 6% colocalization, thus including nanoparticles that did not reach the lysosomes. The side scattering depends on the size of the object, but also on the material (refractive index) and its complexity. Given their bigger size and larger content, it is expected for the lysosomes to have higher VSSC than the early-vesicles in which nanoparticles are internalized and trafficked, such as the endosomes.

As an additional control, in order to determine whether some of the low VSSC objects could also be free nanoparticles, such as, for instance, nanoparticles not properly washed away from the cellular membrane, carried over during the organelle extraction, we extracted organelles from cells exposed to nanoparticles after energy depletion with sodium azide (NaN_3) (Figure S8, Supporting Information). Nanoparticle uptake is energy-dependent.[24] Thus, in energy-depleted cells, after washing away the extracellular nanoparticles and extracting the organelles, we should not detect any nanoparticles. The results showed that in energy-depleted conditions only <5% fluorescent events could be detected compared to what was recovered after the same exposure time in normal conditions, when uptake is present. Thus ≈95% of the fluorescent objects detected in standard conditions are indeed nanoparticles enclosed in organelles. The observed drop in fluorescent events in energy-depleted cells also suggested that the measured fluorescence came from nanoparticles actively internalized and trafficked into different organelles, and eventual free dye leaking from the nanoparticles and passively diffusing inside the cells and into the organelles, if present at all, was anyway washed away in the different steps for organelle extraction prior to measurement.

2.5. Organelle Flow Cytometry for Kinetics of Intracellular Trafficking

Having confirmed the suitability of organelle flow cytometry to quantify nanoparticle colocalization with specific cell organelles over time, we then used the method to determine the effect of nanoparticle size on the kinetics of arrival to lysosomes. **Figure 6** shows lysosome colocalization kinetics in cells exposed to 40, 100, and 200 nm PS-COOH nanoparticles. Given their different size, cells were exposed to different concentrations of the three nanoparticle sizes in order to obtain comparable number of fluorescent organelles at the same exposure time. The smaller nanoparticles (40 and 100 nm) had a similar trend and showed faster trafficking to the lysosomes than the 200 nm nanoparticles. After 5-h chase, 50% of the

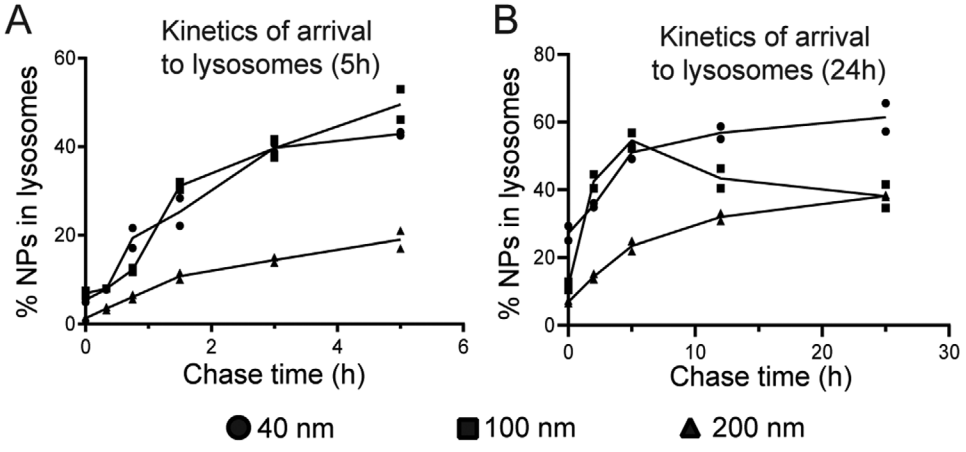

Figure 6. Kinetics of trafficking to the lysosomes for nanoparticles of different sizes. Nanoparticle colocalization with LAMP1-stained lysosomes over time is determined from organelles recovered from HeLa cells exposed to fluorescent green PS-COOH nanoparticles (FITC) of different sizes (20, 100, and 200 μg mL^{-1} for the 40, 100, and 200 nm nanoparticles, respectively). Fraction of nanoparticles in the lysosomes after A) 30-min pulse and different chase times up to 5 h or B) 1-h pulse and different chase times up to 24 h. For all nanoparticle sizes accumulation into the lysosomes over time is observed. The smaller nanoparticles (40 and 100 nm) show faster kinetics than the 200 nm. Over longer chase time, for the 40 nm nanoparticles accumulation in the lysosomes increases up to ≈60%, whereas for the 100 nm nanoparticles a slight decrease is observed. For the 200 nm nanoparticles, a linear increase up to only ≈35% after 24 h is observed. The total number of objects measured in all organelle fractions recovered from 2 replicate samples is shown together with a line that passes through their average.

40 and 100 nm nanoparticles were already in the lysosomes, as opposed to only 20% for 200 nm (Figure 6A). When extending the chase time to 24 h after 1-h pulse (Figure 6B), the results for the early chase times were highly reproducible, while at longer chase times, different trends were observed. For the 40 nm nanoparticles, a clear plateau at roughly 60% colocalization was reached after around 12-h chase. For the 100 nm nanoparticles, instead, after reaching around 50% colocalization after 5 h, a moderate decrease in colocalization was observed, which could indicate a more complex behavior. Finally, for the 200 nm nanoparticles, even after 24-h chase a steady increase in colocalization up to only 35% was observed, suggesting slower uptake and intracellular trafficking or possibly trafficking into different organelles. In agreement with our results, previous works have also shown that a fraction of nanoparticles seems to never reach the lysosomes.[4,25] Determining where these nanoparticles are and why they are processed differently by cells remains an important question for the field to be answered. Overall, the results showed that changing nanoparticle size affects both the intracellular trafficking kinetics as well as the percentage of nanoparticles reaching the lysosomes. As a further control, the same experiments were performed at 4 °C (Figure S9, Supporting Information) in order to stop intracellular trafficking:[31] as expected, no increase in nanoparticle colocalization with the lysosomes was observed, confirming that the observed variations in colocalization in standard conditions were due to intracellular trafficking to the lysosomes.

Finally, we noted that thanks to their larger size thus stronger signal, for the 200 nm nanoparticles we could precisely distinguish between organelles containing one, two, or more nanoparticles (**Figure 7**A). This is demonstrated by the linear proportionality in the median fluorescence of these populations (Figure 7B). Therefore, it was also possible to study the distribution of the number of nanoparticles per organelle as they were trafficked to the lysosomes. The results in Figure 7C showed that the fractions of organelles with 1 nanoparticle decreased over time, while the organelles with more than 1 nanoparticle increased, as expected when more nanoparticles are trafficked in the same organelles. Similar results could be obtained also for the 100 nm nanoparticles when labeled

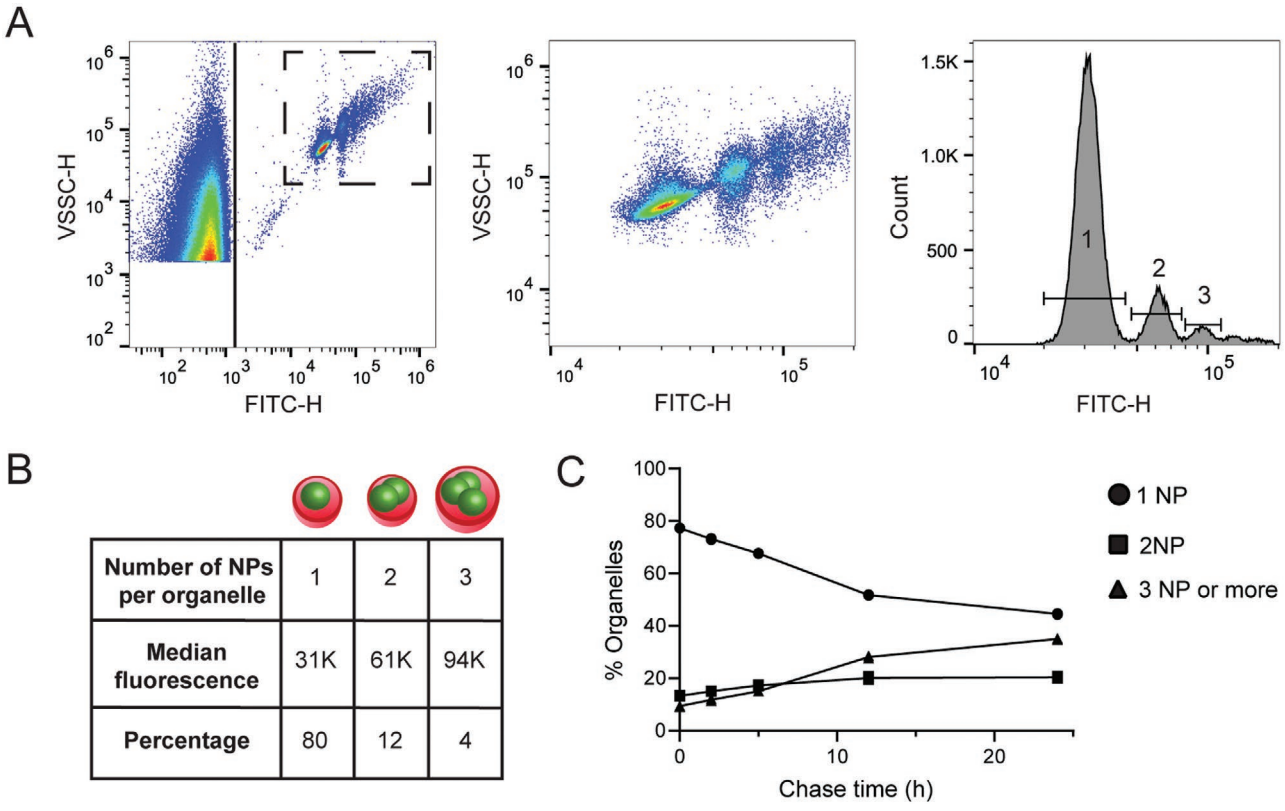

Number of NPs per organelle	1	2	3
Median fluorescence	31K	61K	94K
Percentage	80	12	4

Figure 7. Quantification of 200 nm nanoparticle number and distribution inside organelles over time. A) Dot plots showing the Violet SSC and FITC fluorescence of organelles extracted from Hela cells exposed for 24 h to 50 μg mL^{-1} 200 nm nanoparticles, reproduced from Figure 2D. The events in the dashed gate are shown at higher magnification in the dot plot in the middle and the corresponding histogram on the right. Several populations can be defined in the nanoparticle channel (FITC), corresponding to organelles containing 1, 2, 3, or more than 3 nanoparticles. B) Median fluorescence of the populations defined in panel A. The proportionality of the fluorescence of the populations defined in panel A shows that the flow cytometer allows to count the exact number of 200 nm nanoparticles inside individual organelles. C) Pulse and chase study of the subpopulations of the organelles containing 200 nm nanoparticles. Hela cells are exposed for 30 min (Pulse) to 200 μg mL^{-1} nanoparticles, and the fractions of organelles containing 1, 2 or more than 2 nanoparticles are determined at different times after removal of the extracellular nanoparticles (Chase). The results show that at increasing chase time, the percentage of organelles with only one nanoparticle decreases while the percentage of those containing more than two nanoparticles increases, suggesting trafficking of more nanoparticles into the same organelles. The results are the total number of objects measured in all fractions recovered from 2 replicate samples, together with a line that passes through their average.

with a red fluorescent dye (Figure S10, Supporting Information), suggesting that with appropriate labels the sensitivity of the method can be further improved also for nanoparticles of smaller sizes. Thus, depending on nanoparticle size, their label properties and intensity, precise information on the number of nanoparticles per organelle and their distribution can be gained. This is an additional level of analysis that cannot be obtained with standard fluorescence imaging or flow cytometry of full cells, where nanoparticle uptake is measured in terms of arbitrary units of cell fluorescence.

As a final step, we tested other procedures for organelle staining and further applications to explore the versatility of the method. Indeed, next to immunostaining with labeled antibodies as we show in Figures 3–6, other methods can be applied to label the organelles of interest. For instance, cells can be transfected with DNA constructs in order to express fluorescently labeled proteins, as commonly done for imaging studies. Figure S11, Supporting Information, shows examples of the results obtained with organelles extracted from cells expressing fluorescently labeled Rab5 (wild type green fluorescent protein labeled Rab5, GFP-Rab5,[32] FITC channel) and clathrin (red fluorescent protein labeled clathrin light chain RFP-Clc,[33] phycoerythrin-Texas Red conjugate (energy coupled dye) channel) (Figures S11A,B and S11C,D, Supporting Information, respectively). The results confirmed that also in this way, fluorescently labeled organelles could be detected, that is, early endosomes labeled by Rab5 and clathrin-labeled organelles. Similarly, after exposure to nanoparticles, the percentage of nanoparticle colocalization with these compartments could be determined. As an example of this, the results showed that after 1 h exposure to 100 nm nanoparticles, around 9% of the organelles containing nanoparticles were labeled by Rab5, consistent with the results obtained by immunostaining with the early endosomal marker EEA1 at comparable time scales (Figure 5D). Thus, by harvesting organelles at different chase times after exposure to nanoparticles, intracellular trafficking kinetics such as those shown in Figure 5 could be determined also in this way. Finally, we also note that using cells expressing fluorescently labeled proteins of interest allows to reduce the sample preparation time, since the organelles of interest are already labeled, thus immunostaining is not required.

At a broader level, while here we focused on organelles involved in intracellular trafficking, any other intracellular compartment can be labeled using antibodies or fluorescently labeled proteins. Similarly, with appropriate labels allowing good detection, as well as good separation in different fluorescence channels, multiple organelles can be labeled in the same cells at the same time, also combining the different labeling methods. As an example of this, Figure S11E–G, Supporting Information, shows results obtained from cells expressing fluorescently labeled GFP-Rab5 to label the early endosomes (FITC channel) and with lysosomes stained with the Cy3-labeled LAMP1 antibody (PE channel). In this way, by repeating the extraction at different times, and using nanoparticles with a label for a different channel, kinetics of intracellular trafficking across different compartments could in principle be determined directly from the same cells (although we did not have a suitable combination to explicitly test this with the available DNA constructs and nanoparticle labels). Nevertheless, the same results can be obtained also by combining different experiments where only one organelle is labeled at each time, as indeed we show in Figure 5D. Both approaches can be followed, overall confirming the versatility of the method and many possible applications.

Finally, while for this study we mainly used polystyrene of different sizes as model nanoparticles in order to validate the method by comparing the results with those obtained with the same nanoparticles by fluorescence imaging, any other nanoparticle can be used, provided it is appropriately labeled, as also any other cell type. As an example of this, Figure S12, Supporting Information, shows results for organelles containing 100 nm negatively-charged liposomes,[34] as an example of a common nanomedicine, as well as silica nanoparticles of different sizes (100 and 200 nm) and different surface functionalization (plain, amino-modified and carboxylated). Thus, after exposure to these nanoparticles, the organelles were harvested for flow cytometry. Similarly to what observed with the polystyrene nanoparticles of different sizes (Figure 2), also in these cases, a population of fluorescently labeled organelles could be distinguished from the background of all unlabeled organelles. This confirmed that the nanoparticle signal was strong enough to allow the detection and quantification of the organelles in which these nanoparticles are trafficked. Indeed, with appropriate labels, the method could be used also to study intracellular trafficking of objects other than nanoparticles and nanomedicines, including for instance viruses, bacteria, pathogens and proteins.

3. Conclusion

Flow cytometry of organelles provides a novel method to generate with ease quantitative data on nanoparticle intracellular distribution and colocalization with specific cell compartments, as well as to determine intracellular trafficking kinetics. This is fundamental information to understand the intracellular behavior of nanomedicines and how by tuning nanoparticle design the outcome at cell level can be affected, thus nanomedicine efficacy improved. The method takes advantage of recent advances in high-sensitivity flow cytometry and the unique properties of nano-sized objects, in particular their high degree of labeling comparing to proteins or other biomolecules. However, with appropriate fluorescent labeling, the method could also be translated to the study of the intracellular trafficking of other biomolecules or objects. Similarly, different methods can be used to tag and detect the organelles of interest, including for instance immuno-staining with labeled antibodies or by extracting organelles from cells expressing fluorescently labeled proteins. Sample preparation could be further optimized by automizing the cell lysis procedure or by extracting organelles from multiple samples in parallel.

In comparison to the current methods to determine colocalization of nanoparticles with specific cell compartments, this method has the advantage of being much faster and offering high-throughput analysis without the need for complex algorithms to determine colocalization from multiple images of individual cells. Thus, it combines the ability of flow cytometry to analyze several thousands of objects with intracellular spatial information, as usually obtained using imaging techniques.

In comparison to live-cell imaging studies, however, the method does not allow to study responses in individual cells, nor to follow the same cells over time in situ. Because of the high throughput and quantitative space and time-resolved information that can be easily obtained, the method could be used as a preliminary tool to test multiple nanomedicines of different design for their intracellular behavior and select the most promising ones. After that, imaging techniques could be used to further characterize their intracellular outcomes in more detail.

Additionally, for nanoparticles with appropriate size and labels, the method allows to count the exact number of nanoparticles contained inside the organelles, which is usually only feasible by electron microscopy. This allows precise quantification of nanoparticle numbers and how their distribution per organelle changes during trafficking. Finally, the method could be extended by using fluorescence-assisted organelle sorting[35] to isolate the organelles in which nanoparticles are trafficked, opening up the possibility to characterize them in more detail, for instance by proteomics.

In conclusion, the presented method takes advantage of the easy high throughput quantification enabled by flow cytometry and constitutes a complementary addition to the existing methods for determining nanoparticle colocalization and intracellular trafficking kinetics, which are mainly based on imaging. The method can be applied by using standard flow cytometers for cell analysis readily available in many laboratories with appropriate high sensitivity settings. Furthermore, novel instruments specifically designed to exploit the high throughput of flow cytometry for the detection and characterization of sub-micrometer objects are being developed to increase sensitivity towards objects of smaller sizes, down to the nanoscale.[36–38] The method presented can be transferred to such instruments, and it would be interesting to test whether the improved sensitivity allows to detect organelles with smaller nanoparticles, or for instance organelles with labeled proteins, which have a lower amount of label per object in comparison to nanoparticles. Similarly, many other applications of organelle flow cytometry and the approaches presented in this work can be foreseen, including in fields other than nanomedicine, as flow cytometers with higher sensitivity are being developed, as well as new methods to further improve fluorescence labeling of the compounds of interest.

4. Experimental Section

Cell Culture: The HeLa cell line (ATCC CCL-2) was maintained in complete cell medium (cMEM), consisting of Eagle's minimum essential medium (MEM) (Gibco, Waltham, MA, USA) supplemented with 10% v/v fetal bovine serum (FBS, Gibco). The cells were passaged when they reached full confluency and cultured at 37 °C and 5% CO_2. All the experiments were performed using cells between passages 2 and 20 after defrosting. Cells were subjected to mycoplasma test once per month to exclude infection.

Characterization of the Nanoparticles: Green (505/515) and red (580/605) fluorescently labeled FluoSpheres carboxylated polystyrene nanoparticles (PS-COOH NPs) were purchased in various sizes (40, 100, and 200 nm) from Invitrogen (Life Technologies, Carlsbad, CA, USA). Different batches of the same nanoparticles were used during this research. Nanoparticle size distribution by DLS and zeta potential were determined using a Malvern Zetasizer Nano ZS. The nanoparticles were dispersed in PBS and cMEM at a concentration of 100 μg mL^{-1}, mixed by pipetting and measured at room temperature, using disposable folded capillary cells (Malvern Instruments Ltd, Worcestershire, UK). Three measurements of 10 runs each were performed for each sample.

Cells Exposure to Nanoparticles: Hela cells were plated at a density 250 000 cells per well in 6-well plates (Greiner Bio-One) 24 h prior to the experiments. Then cells were exposed to the yellow-green fluorescent PS-COOH nanoparticles at a concentration of 20, 100, and 200 μg mL^{-1}, for the 40, 100, and 200 nm samples respectively, in cMEM. These cell densities and nanoparticle concentrations were used in all the experiments unless specified otherwise. Given the different nanoparticle size, different nanoparticles concentrations were used in order to obtain a comparable number of fluorescent events after organelle extraction.

Pulse and Chase Experiments: In the pulse and chase experiments, Hela cells seeded as described above were exposed to the nanoparticles for 30 min (short kinetics) or 1 h (long kinetics) pulse. After that, cells were washed with cMEM (2 mL) three times and PBS five times to help removing any nanoparticle adsorbed on the cell surface or in the wells. Next, the cells were further incubated in fresh cMEM (chase) and the cells and organelles were extracted at different chase times. An additional pulse and chase experiment was performed as a control for the method, consisting of a 30-min pulse followed by a chase at 4 °C and extracting the organelles at different chase times. In all the experiments, two replicate samples were prepared for each time-point.

Sodium Azide Experiments: In order to deplete cell energy, before exposure to the nanoparticles, the cells were incubated with cMEM supplemented with sodium azide (NaN_3) (6688, Merck) at a concentration of 10 mg mL^{-1} for 1 h. Then, cells were exposed to the nanoparticles for 30 min in cMEM supplemented with NaN_3. As a control for each nanoparticle size, an additional sample was prepared, for cells exposed to the same nanoparticles in standard conditions (without sodium azide). Next, the cells were washed with cMEM (2 mL) three times and PBS five times, the organelles were extracted, and the number of fluorescent objects detected by flow cytometry in standard conditions and energy-depleted cells were compared. Two independent experiments were performed, each containing duplicate samples for all conditions.

Organelle Extraction: At the time of extraction, the cells were washed with cMEM one time and PBS two times. The cells were collected by adding trypsin-ethylenediaminetetraacetic acid (EDTA) (0.05% v/v) for 5 min at room temperature, centrifuged (200 g, 5 min) and the pellet was resuspended in PBS. Intact cells were measured by flow cytometry or organelles were extracted as follows.

The cells were centrifuged a second time (200 g, 5 min), and the pellet was resuspended in a lysis buffer consisting of 5 mM Tris-Base, 1mM EDTA supplemented with a tablet of protease inhibitor cocktail (Sigma-Aldrich St Luis, USA) (1 tablet for 15 mL of lysis buffer). Roughly 0.5 mL of lysis buffer per each 1×10^6 cells was used. From this step onwards, all steps were performed at 4 °C. Cells were lysed with a Potter-Elvehjem homogenizer. The cells were counted using a hematocytometer after staining with Trypan Blue before and after lysis to assess the lysis percentage. All experiments were performed in a regime between 65 and 85% lysis (usually around 5 strokes). Next, the organelle mixture was centrifuged at 1 500 g for 10 min to remove the cell debris and nuclei. The pellet was discarded and the supernatant was transferred to a clean tube. At this point, the organelle fractions were ready to be analyzed in the flow cytometer. If necessary, immunostaining of the organelles was performed as described below.

For lysing cells using glass beads, a scoop of 1 mm glass beads (11 079 110, BioSpecproduct), (approximately 400 μL), was added to a tube containing a sample of organelles extracted from 1×10^6 Hela cells. Then, the sample was kept at 3 000 rpm for 60 s in a Mini-Beadbeater-24 (BioSpecproducts). The lysis efficiency was assessed by counting with Trypan Blue as described above.

Immunostaining of Organelles for Flow Cytometry: The fluorescently labeled antibody against EEA1 (Early endosome antigen 1) (PE-conjugated, Sc-137130) was purchased from Santa Cruz (Dallas,

USA) and those against LAMP1 (Lysosomal-associated membrane protein 1) with lumenal (PE.Cy5 conjugated, ab25222) and cytosolic epitopes (Cy3 conjugated, L0419) were purchased from BD Biosciences (Erembodegem, Belgium) and Sigma-Aldrich (St Luis, USA), respectively. The lysosomal lumenal antibody was used only for the optimization of the extraction of the organelles to count the number of damaged lysosomes. The cytosolic antibody was used for all the pulse and chase experiments. All antibodies were incubated with the extracted organelles at dilution 1:200 in a final volume of 200 µL for 3 h at room temperature. The free antibody was removed by size exclusion chromatography in a 10 cm and 15 mL Sepharose CL-4B gravity column (10 273 151, Sigma-Aldrich St Luis, USA). One mL of the organelles sample was loaded in the column and after the whole sample had entered the column, PBS was added until the column was filled (approximately 10 mL) and the organelles were eluted in 0.5 mL fractions. A minimum of 15 fractions were recovered. All eluted fractions were measured by flow cytometry for 30 s at 10 µL min^{-1}. When necessary, the sample was diluted in PBS to lower the amount of events per second in order to avoid swarm detection. The organelles were usually eluted between the 6th and 10th fractions. The free antibody and proteins were usually eluted between the 14th and 20th fractions. The removal of free antibody was assessed by measuring the fluorescence at 569 nm of all the eluted fractions in a spectro-fluorometer (Molecular Devices, CA, USA). The removal of the free proteins from the cytosol was checked by calculating the protein concentration of the eluted fractions using the Micro bicinchoninic acid (BCA) Protein Assay Kit (Thermofisher Scientific, Waltham, MA, USA) following the manufacturer's instructions. Alternatively, in order to determine the integrity of the lysosomes and the washing efficiency of the nanoparticles, and for the pulse and chase experiment at 4 °C and the western blot studies, organelles were spun down a 20 000 g for 20 min and the pellet and supernatant were further analyzed.

Setting up the Flow Cytometer for High Sensitivity Measurements: A Cytoflex flow cytometer model S (Beckman Coulter, Pasadena, CA) equipped with 4 lasers (405, 488, 561, 605 nm) was used for all the measurements (unless specified). The Violet Side Scattering height (VSSC-H) was selected as threshold to block background events and was set up to 1500. The detailed acquisition settings for the different nanoparticles and dyes are indicated in Table S1, Supporting Information. PBS was measured at slow flow rate (10 µL min^{-1}) to assess the amount of noise measured in the samples. A maximum of 200 events per second (eps) was allowed. If after 5 min measuring PBS the events per second measured were higher than 200, the VSSC gain was lowered. Next, the Megamix mixture was measured at slow speed (10 µL min^{-1}) to calibrate the instrument. The Megamix mixture was prepared by adding the Megamix-Plus FSC and the Megamix-Plus SSC (catalog numbers 7802 and 7803, Biocytex, Marseille, France) in a 1:1 ratio and final volume of 200 µL. Both solutions contain a mix of different size fluorescent beads on the FITC channel: 100, 300, 500, and 900 nm for Megamix-FSC; and 160, 200, 240, and 500 nm for Megamix-SSC. For organelle samples stained with the LAMP1 antibodies that had fluorescent dyes emitting in channels other than the FITC (thus the PerCP or the PE channels for the lumenal and cytosolic LAMP1 immunostained lysosomes respectively), the gain values had to be optimized independently. This was performed by measuring an organelle sample without and with LAMP1 staining and by adjusting the gain until a maximum separation in fluorescence between the unstained and stained samples was achieved. The optimal gain was set at around 1000 for both channels. Next, an inclusive threshold (logical operator "OR") was also added in the same channels to help detect any lysosome with too low side scattering in VSSC-H. This was performed again by measuring an organelle sample without LAMP1 staining and by lowering the threshold in the lysosome channel until background events appeared. The optimal PerCP-H or PE-H threshold was set at around 2000. Additionally, for the 40 nm nanoparticles, the gain in the FITC channel also had to be optimized and was set at 1000, because the settings optimized based on the Megamix calibration beads did not separate well the nanoparticle population from the background. For these nanoparticles, next to the threshold in VSSC-H, an inclusive threshold (logical operator "OR") was also set in the FITC-H channel and set at around 2000 in order to detect and measure also fluorescent events with too low VSSC-H. All the samples were measured at slow flow rate (10 µL min^{-1}) and between 1500 and 3500 events per second (eps). The samples were diluted in PBS, when necessary, to reach the desired concentration and were run for 1 min until the eps became stable, before proceeding to record the events. Data was acquired using CytExpert 2.0 software (Beckman Coulter) and analyzed using Flowjo software version 10.7.1 (BD Biosciences, San Jose, CA).

Nanoparticle Count at the Flow Cytometer: The number of yellow-green fluorescent carboxylated polystyrene nanoparticles (PS-COOH) per µL in the nanoparticle stocks was calculated for all the sizes using the concentration of the nanoparticles given by the manufacturer (based on polystyrene density, the stock concentration was calculated as 52.5 mg mL^{-1} for the 40 nm and 21 mg mL^{-1} for the 100 and 200 nm, corresponding to 1.5×10^{12}, 3.8×10^{10}, and 4.8×10^{9} nanoparticles per µL for the 40, 100, and 200 nm nanoparticles, respectively). From the stock, dilutions at 1.5×10^{4}, 3.8×10^{3}, and 4.8×10^{3} nanoparticle per µL, respectively for the 40, 100, and 200 nm nanoparticles were prepared. Three samples were prepared for each size as replicates. All samples were measured by flow cytometry at 30 µL min^{-1} for a total of 60 s each and the total number of nanoparticles was determined, after gating the nanoparticles based on their fluorescence. The nanoparticle events in the flow cytometer were gated by using PBS as a negative control to exclude background events.

Western Blot Analysis: For western blot analysis, Hela cells were seeded at a density of 1×10^{7} cells in a T175 cm^2 flask (Greiner) 24 h prior to the experiment. The cells were extracted by adding trypsin-EDTA (0.05% v/v) for 5 min at room temperature and centrifuged at 200 g for 5 min. The pellet was resuspended in PBS (10 mL) and centrifuged again at 200 g for 5 min. The pellet was then resuspended in lysis buffer (4 mL) supplemented with protease inhibitor prepared as described above. The cell debris and nuclei were removed by centrifuging at 1 500 g for 10 min and collecting the supernatant. The supernatant was divided into 4 samples, which were subjected to different lysis methods. The Potter-Elvehjem homogenizer was used to prepare samples at 45%, 75%, and 100% lysis. The lysis efficiency was assessed by counting the number of cells with Trypan Blue as explained above. The 4th sample was subjected to lysis with 1 mm glass beads (11 079 110, BioSpecproduct), as described above.

After lysis, the organelles were centrifuged at 20 000 g for 20 min for all the samples. Both supernatant and pellet were recovered for further analysis. The pellet was centrifuged an extra time at 20 000 g for 20 min to further wash any free proteins. The protein amount in the samples was determined using the Micro BCA Protein Assay Kit (Thermofisher Scientific, Waltham, MA, USA) following the manufacturer's instructions. For each sample, 12 µg of proteins were loaded on a 10% acrylamide sodium dodecyl sulfate polyacrylamide gel electrophoresis gel and transferred to a polyvinylidene fluoride membrane. The membrane was blocked with 5% milk powder (w/v) in 1× tris buffered saline (TBS) containing 0.1% Tween 20 (v/v) for 2 h at room temperature. Next, the membrane was incubated overnight at 4 °C with primary antibodies diluted 1:1000 in the blocking solution. The primary antibodies used were: anti-LAMP1 (555 798, BD Biosciences) and anti-Cathepsin D (610 801, BD Biosciences) both against human. The membrane was washed three times for 10 min with TBS containing 0.1% Tween 20 (v/v), and subsequently incubated for 2 h at room temperature with a HRP-conjugated (horseradish peroxidase) secondary antibody against mouse (1:2000, P0447, DAKO). The bound antibody was detected by using the Pierce ECL Plus Substrate (Thermofisher Scientific, Waltham, MA, USA) following the manufacturer's instructions and images were taken using ChemiGenius II bioimaging system.

Supporting Information

Supporting Information is available from the Wiley Online Library or from the author.

Acknowledgements

This work was funded by the European Research Council (ERC) under the European Union's Horizon 2020 Research and Innovation Programme under grant agreement no. 637614 (NanoPaths). A.S. kindly acknowledges the University of Groningen for additional funding (Rosalind Franklin Fellowship). S.D. was supported by a postdoctoral fellowship granted by the Research Foundation Flanders (FWO) and the Flemish Institute for Technological Research (VITO) under grant agreement 12S6517N. J. Smit (Department of Medical Microbiology and Infection Prevention, University Medical Center Groningen) is kindly acknowledged for providing the construct to express Rab5-GFP.

Conflict of Interest

The authors declare no conflict of interest.

Author Contributions

H.G.R. designed and performed all experiments, analyzed and interpreted the data and wrote the manuscript. S.D. contributed to the optimization of the flow cytometry setting for the measurements of nano-sized objects and revised the manuscript. A.S. conceived and designed the experiments, analyzed and interpreted the data, and wrote the manuscript.

Data Availability Statement

The data that support the findings of this study are available from the corresponding author upon reasonable request.

Keywords

endocytosis, high sensitivity flow cytometry, intracellular trafficking, nanomedicine, nanoparticles, organelle flow cytometry, organelles

Received: February 11, 2021
Revised: June 15, 2021
Published online: July 17, 2021

[1] L. M. Bareford, P. W. Swaan, *Adv. Drug Delivery Rev.* **2007**, *59*, 748.
[2] M. Ferrari, *Nat. Rev. Cancer* **2005**, *5*, 161.
[3] D. Peer, J. M. Karp, S. Hong, O. C. Farokhzad, R. Margalit, R. Langer, *Nat. Nanotechnol.* **2007**, *2*, 751.
[4] D. Vercauteren, H. Deschout, K. Remaut, J. F. J. Engbersen, A. T. Jones, J. Demeester, S. C. De Smedt, K. Braeckmans, *ACS Nano* **2011**, *5*, 7874.
[5] P. H. Hemmerich, A. H. von Mikecz, *PLoS One* **2013**, *8*, e62018.
[6] V. Levi, E. Gratton, *Cell Biochem. Biophys.* **2007**, *48*, 1.
[7] J. W. D. Comeau, S. Costantino, P. W. Wiseman, *Biophys. J.* **2006**, *91*, 4611.
[8] R. Heintzmann, T. Huser, *Chem. Rev.* **2017**, *117*, 13890.
[9] E. Betzig, G. H. Patterson, R. Sougrat, O. W. Lindwasser, S. Olenych, J. S. Bonifacino, M. W. Davidson, J. Lippincott-Schwartz, H. F. Hess, *Science* **2006**, *313*, 1642.
[10] H. Lin, S. P. Centeno, L. Su, B. Kenens, S. Rocha, M. Sliwa, J. Hofkens, H. Uji-I, *ChemPhysChem* **2012**, *13*, 973.
[11] S. W. Hell, J. Wichmann, *Opt. Lett.* **1994**, *19*, 780.
[12] I. Tavernaro, C. Cavelius, H. Peuschel, A. Kraegeloh, *Beilstein J. Nanotechnol.* **2017**, *8*, 1283.
[13] E. N. M. N. t. Hoen, E. J. van der Vlist, M. Aalberts, H. C. H. Mertens, B. J. Bosch, W. Bartelink, E. Mastrobattista, E. V. B. van Gaal, W. Stoorvogel, G. J. A. Arkesteijn, M. H. M. Wauben, *Nanomedicine* **2012**, *8*, 712.
[14] I. Fialka, P. Steinlein, H. Ahorn, G. Böck, P. D. Burbelo, M. Haberfellner, F. Lottspeich, K. Paiha, C. Pasquali, L. A. Huber, *J. Biol. Chem.* **1999**, *274*, 26233.
[15] D. Rajotte, C. D. Stearns, A. K. Kabcenell, *Cytometry, Part A* **2003**, *55A*, 94.
[16] A. Schneider, S. Kurz, K. Manske, M. Janas, M. Heikenwälder, T. Misgeld, M. Aichler, S. F. Weissmann, H. Zischka, P. Knolle, D. Wohlleber, *Sci. Rep.* **2019**, *9*, 8492.
[17] M. Degtyarev, M. Reichelt, K. Lin, *PLoS One* **2014**, *9*, e87707.
[18] E. J. van der Vlist, E. N. M. Nolte-'t Hoen, W. Stoorvogel, G. J. A. Arkesteijn, M. H. M. Wauben, *Nat. Protoc.* **2012**, *7*, 1311.
[19] J. A. Welsh, J. A. Holloway, J. S. Wilkinson, N. A. Englyst, *Front. Cell Dev. Biol.* **2017**, *5*, 78.
[20] A. Morales-Kastresana, B. Telford, T. A. Musich, K. McKinnon, C. Clayborne, Z. Braig, A. Rosner, T. Demberg, D. C. Watson, T. S. Karpova, G. J. Freeman, R. H. Dekruyff, G. N. Pavlakis, M. Terabe, M. Robert-Guroff, J. A. Berzofsky, J. C. Jones, *Sci. Rep.* **2017**, *7*, 1878.
[21] Y. Tian, M. Gong, Y. Hu, H. Liu, W. Zhang, M. Zhang, X. Hu, D. Aubert, S. Zhu, L. Wu, X. Yan, *J. Extracell. Vesicles* **2020**, *9*, 1697028.
[22] L. Ma, S. Zhu, Y. Tian, W. Zhang, S. Wang, C. Chen, L. Wu, X. Yan, *Angew. Chem., Int. Ed.* **2016**, *55*, 10239.
[23] C. Chen, K. Gao, H. Lian, C. Chen, X. Yan, *Biosens. Bioelectron.* **2019**, *131*, 185.
[24] A. Salvati, C. Åberg, T. dos Santos, J. Varela, P. Pinto, I. Lynch, K. A. Dawson, *Nanomedicine* **2011**, *7*, 818.
[25] P. Sandin, L. W. Fitzpatrick, J. C. Simpson, K. A. Dawson, *ACS Nano* **2012**, *6*, 1513.
[26] J. A. Kim, C. Aberg, A. Salvati, K. A. Dawson, *Nat. Nanotechnol.* **2012**, *7*, 62.
[27] M. J. McVey, C. M. Spring, W. M. Kuebler, *J. Extracell. Vesicles* **2018**, *7*, 1454776.
[28] A. Spittler, *Set-Up of the CytoFLEX for Extracellular Vesicle Measurement, Application Note*, pp. 1–7, https://www.mybeckman.nl/flow-cytometry/instruments/cytoflex.
[29] E. Van Der Pol, M. J. C. Van Gemert, A. Sturk, R. Nieuwland, T. G. Van Leeuwen, *J. Thromb. Haemostasis* **2012**, *10*, 919.
[30] M. S. Islam, A. Aryasomayajula, P. R. Selvaganapathy, *Micromachines* **2017**, *8*, 83.
[31] E. L. Punnonen, K. Ryhänen, V. S. Marjomäki, *Eur. J. Cell Biol.* **1998**, *75*, 344.
[32] H. M. Van Der Schaar, M. J. Rust, H. V. D. E.-M. Chen, J. Wilschut, X. Zhuang, J. M. Smit, *PLoS Pathog.* **2008**, *4*, e1000244.
[33] A. Tagawa, A. Mezzacasa, A. Hayer, A. Longatti, L. Pelkmans, A. Helenius, *J. Cell Biol.* **2005**, *170*, 769.
[34] K. Yang, B. Mesquita, P. Horvatovich, A. Salvati, *Acta Biomater.* **2020**, *106*, 314.
[35] D. J. Gauthier, J. A. Sobota, F. Ferraro, R. E. Mains, C. Lazure, *Proteomics* **2008**, *8*, 3848.
[36] S. Zhu, L. Yang, Y. Long, M. Gao, T. Huang, W. Hang, X. Yan, *J. Am. Chem. Soc.* **2010**, *12176*, 132.
[37] L. Yang, S. Zhu, W. Hang, L. Wu, X. Yan, *Anal. Chem.* **2009**, *81*, 2555.
[38] S. Zhu, L. Ma, S. Wang, C. Chen, W. Zhang, L. Yang, W. Hang, J. P. Nolan, L. Wu, X. Yan, *ACS Nano* **2014**, *8*, 10998.